Available online at www.sciencedirect.com
ScienceDirect
Journal of the European Ceramic Society 28 (2008) 935–942
www.elsevier.com/locate/jeurceramsoc

Fabrication and some properties of textured alumina-related compounds by colloidal processing in high-magnetic field and sintering

Yoshio Sakka*, Tohru S. Suzuki, Tetsuo Uchikoshi

Nano Ceramics Center, National Institute for Materials Science, 1-2-1 Sengen, Tsukuba, Ibaraki 305-0047, Japan

Available online 25 October 2007

Abstract

Recently to improve properties, highly microstructure controlled ceramics such as fine-grained, textured and laminated structures are required. We have demonstrated a new processing of textured ceramics with a feeble magnetic susceptibility by colloidal processing in a high-magnetic field and subsequent heating. As colloidal processing, slip casting and electrophoretic deposition (EPD) have been conducted successfully. Colloidal processing is known to be a powerful method for consolidating fine particles with a high density and homogeneous microstructure. Crystalline-textured controlled laminated alumina can be fabricated using EPD by varying the angle between the vectors of electric field and magnetic field. Also textured ceramics with complicated structure such as β-alumina and alumina-based nanocomposite can be fabricated by reaction sintering. The textured alumina-related compounds showed anisotropic properties depending on the crystal plane. The colloidal processing in a high-magnetic field confers several advantages and can be applied to many non-cubic ceramics.

Keywords: Textured ceramics; Alumina; Slip casting; Magnetic field; EPD

1. Introduction

The controlled development of texture is one of the ways for effective in improving the physical and mechanical properties.[1] Several approaches have been developed to produce textured ceramics, including: (i) the template grain growth (TGG) method, which involves the alignment of a small fraction of large rod-like particles in a fine powder matrix during forming by tape casting or extrusion.[1,2] During subsequent sintering, these template grains grow and consume the matrix grains to produce textured microstructure; (ii) the hot-working method, which involves the imposition of a uniaxial stress on the loosely packed powder or green powder compacts during sintering.[3,4] The texture development is essentially attributed to the elongated grain rotation induced by shear strain and the grain alignment is either parallel or perpendicular to the plane strain, depending on the tensile or compressive strain; (iii) the magnetic field alignment method, which uses a magnetic field to align the ceramic particles in a suspension during the colloidal processing, and the strong texture could be developed during subsequent sintering.[5,6] The principle of the process is that a crystal with an anisotropic magnetic susceptibility will rotate to an angle minimizing the system energy when placed in a magnetic field.[6] The magnetic torque T attributed to the interaction between the anisotropic susceptibility and a magnetic field is estimated by the following equation:

$$T = -\frac{\Delta\chi V B^2 \sin 2\theta}{2\mu_0} \quad (1)$$

where $\Delta\chi$ ($=|\chi_{a,b} - \chi_c|$) is the anisotropy of the magnetic susceptibilities which are measured for the a, b-axis ($\chi_{a,b}$) and c-axis (χ_c), V the volume of the materials, B the applied magnetic field, θ the angle between an easy magnetization axis in a crystal and imposed magnetic field direction, and μ_0 is the permeability in a vacuum. This magnetic torque is the driving force for the magnetic alignment. However, since the anisotropy of the magnetic susceptibilities of feeble magnetic materials are very small,[7,8] even in an applied high-magnetic field the magnetic torque is small; therefore, to align each particle special attention should be paid.

We have demonstrated that the highly textured microstructure of dense alumina can be fabricated by colloidal processing in a strong magnetic field, followed by heating,[5] and that this process is applied for alumina-based composites.[6] As the colloidal processing, slip casting and electrophoretic deposition (EPD)

* Corresponding author. Tel.: +81 29 859 2461; fax: +81 29 859 2401.
E-mail address: SAKKA.Yoshio@nims.go.jp (Y. Sakka).

0955-2219/$ – see front matter © 2007 Elsevier Ltd. All rights reserved.
doi:10.1016/j.jeurceramsoc.2007.09.039

were conducted.[9] Requirements for obtaining textured ceramics by slip casting in a high-magnetic field and sintering are as follows[6]: (1) the particle should be single crystal and well dispersed; (2) crystal structure should be non-cubic to yield an anisotropic magnetic susceptibility; (3) magnetic energy should be larger than thermal motion energy; (4) the viscosity of the suspension should be low enough to rotate the particles with a low energy; (5) grain growth is necessary to obtain a highly oriented structure especially when spherical particles are used. In general, non-cubic materials have anisotropic susceptibilities attributable to asymmetry. It is possible for this type of processing (slip casting in a strong magnetic field, followed by heating) to be applied to other non-cubic ceramics such as TiO_2, AlN, ZnO, SnO_2, hydroxyapatite, Si_3N_4, bismuth titanate, mesoporous silica, etc.[5,6,10–22] This technique is also applied for fabrication of the textured alumina-based composites, such as alumina–SiC,[23] alumina–zirconia,[24] etc.

Here, we demonstrate that textured ceramics with complicated structure such as β-alumina and alumina-based nanocomposites can be fabricated by the combination of above technique and reaction sintering β-alumina is known to be a Na^+ ionic conductor and it used in the Na–S battery.[25,26] However, the polycrystalline β-alumina has conduction planes that are randomly oriented. Therefore, the ionic conductivity of this polycrystalline material is lower than that of a single crystal. If it is possible to prepare a texture developed β-alumina polycrystallite, β-alumina with a high-ion conductively is expected. Alumina-based ceramics are known to show good mechanical properties, but their strength is low at high temperatures.[27,28] Mullite is considered to be a candidate ceramic for high-temperature structural applications because of its excellent high-temperature properties.[29,30] We have reported that Al_2O_3–mullite–SiC nanocomposites can be prepared by partial oxidation–reaction sintering of the Al_2O_3–SiC green body.[31] Our objective is to prepare textured nanocomposites that have better mechanical properties than the mullite single phase, and a flexural strength at high temperature better than Al_2O_3 and SiC.

In this paper, fabrication of textured β-alumina and Al_2O_3–mullite–SiC nanocomposites with complicated structure are demonstrated by slip casting in a high-magnetic field and reaction sintering. Then, the EPD in a high-magnetic field to obtain textured laminated alumina are shown. Some isotropic properties of the textured ceramics are also demonstrated.

2. Experimental

2.1. Textured β-alumina

α-Alumina powders with an average particle size of 0.2 μm (Sumitomo Chemical Co. Ltd., AKP-50) were used. Sodium formate (HCOONa, Kanto Chemical) and magnesium acetate tetrahydrate ($(CH_3COO)_2Mg{\cdot}4H_2O$, Kanto Chemical) were used as the sources of the Na_2O and MgO, respectively.[32,33] Monodispersed spherical polymethyl metacrylate (PMMA) particles with an average particle size of 0.15 μm (Soken Chemical Co. Ltd., MP-1451) were used to increase the pores of the green bodies. [34,35] Aqueous dispersed suspension of α-alumina powder with 30 vol.% solids were prepared by adding the appropriate amount of poly-(ammonium)acrylate (Toagosei Co. Ltd., A-6114).[36] For samples with added polymer, a polymer with 10 vol.% solids was added at that time. After ultrasonic irradiation,[36] the suspensions were slip casted in 10 T, where the direction of the magnetic field was parallel to the casting direction. The prepared green bodies were calcined at 1073 K for 2 h to provide enough strength for handling during the following infiltration treatment and to decompose and evaporate the polymer. An aqueous solution of sodium formate and magnesium acetate, prepared in an approximately 80–90% saturated solution, were then infiltrated into the pores of the calcined α-alumina compacts. The alumina compacts containing Na^+ and Mg^{2+} were heated at the rate of 8 K min^{-1} to 1073 K for 2 h in air. Na_2O is a component of β-alumina and promotes the densification by the liquid phase, and MgO increases the thermal stability of the β-alumina at high temperature.[32] The obtained samples were embedded in the produced powdered alumina to prevent the loss of Na_2O and sintered at 1973 K for 2 h in air. The appearance and orientation of the β-alumina were confirmed by X-ray diffraction (XRD). The ionic conductivity was determined by complex impedance method.

2.2. Textured alumina–mullite–SiC nanocomposite

α-Al_2O_3 powder (Taimei Chemical: TM-DAR) with 0.15 μm in diameter and β-SiC powder (Ibiden Co. Ltd.) with 0.27 μm in diameter were used as the starting powders. Aqueous suspensions with a solid content of 30 vol.% were prepared. The SiC powder content of each colloidal suspension was fixed at 5, 10 and 15 vol.%, and each one after consolidation was labeled T-5SiC, T-10SiC and T-15SiC, respectively. The powder mixtures were dispersed with an appropriate amount of polyelectrolyte (polyammoniumacrylate, A-6114, Toagosei Co.). After ultrasonic vibration was applied to facilitate dispersion of the powder agglomerates,[36] slip casting was done with and without a high-magnetic field (12 T). In some case, beads-milling (Kotobuki Industry Co. Ltd.: UAM015) using zirconia beads of 0.05 mm in diameter was conducted to the deagglomeration of SiC fine powders.[37]

Fig. 1 shows schematic of partial oxidation and reaction sintering. This process offers several advantages: (1) it eliminates the need to reduce the particle size of the inclusion phase to

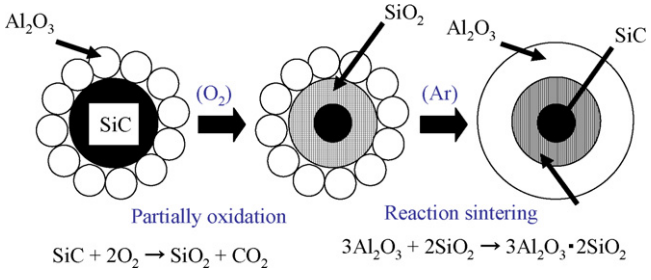

Fig. 1. Schematic diagram for partial oxidation and reaction sintering.

the nanometer range by milling and thus provides better control in minimizing impurities; (2) because of volume increase during reaction sintering, sintering shrinkage are lower. The partial oxidation treatment was conducted in an alumina crucible in a stream of O_2 at 1473 and 1573 K for 1 h. Reaction sintering was then carried out in a stream of Ar at 1873 K for 2 h. The partial oxidation treatment and reaction sintering were continuously conducted. The partial oxidation condition was confirmed in advance by a thermogravimetric analysis.

The phases and texture analyses were done by analyzing the XRD. The resulting microstructures were observed by SEM and TEM. The samples were cut and ground using a diamond wheel into 4 mm × 3 mm × 20 mm bars for the three-point bending test. The mechanical properties of the samples were evaluated by the three-point bending with a span 16.1 mm and a crosshead speed of 0.5 mm min^{-1}.

2.3. Textured laminated alumina by EPD in magnetic field

Aqueous alumina suspension of 0.2 μm in diameter with 10 vol.% solid content was prepared adjusting the pH 4. EPD was conducted in 10 T at a constant voltage of 30 V at room temperature. A Pd sheet was used as the cathodic substrate to absorbed hydrogen evolved by the electrolysis of water.[38] The direction of the electric field relative to the magnetic field (the angle between the vector **E** and **B**) was altered (0°, 45° and 90°) to control the dominant crystal faces.[39] After the EPD for 50 min, the thickness of the compacts was approximately 6 mm. After CIP treatment at 392 MPa, the compacts were sintered at 1873 K for 2 h in air. The bend strength was determined using the three-point bending test with a span length of 18 mm and a crosshead speed of 0.5 mm min^{-1}.

3. Results and discussion

3.1. Textured β-alumina

The textured porous α-alumina bodies were prepared by the slip casting of well-dispersed α-alumina suspensions followed by heating at 1073 K. The relative density of the calcined bodies without polymer addition was 60.7%, but that with the polymer addition[34] decreased to 55%. The porous alumina bodies were analyzed for Na and Mg in the initial compositions (molar ratio) of Na_2O:MgO:Al_2O_3 = 0.25:0.1:1.0. After infiltration and calcination, the molar ratio of Na_2O:MgO:Al_2O_3 for the calcined compacts were calculated from the weight loss. The results of the infiltrated amounts in the pores of the α-alumina compacts were Na_2O:MgO:Al_2O_3 = 0.12–0.2:0.019–0.024:1 for the samples without the polymer addition, and Na_2O:MgO:Al_2O_3 = 0.22–0.3:0.022–0.024:1 for the samples with the polymer addition.

Fig. 2 shows the XRD patterns of the infiltrated porous bodies initially with and without polymer addition and reaction sintering at 1973 K. The sample was confirmed to be β-alumina by the reaction of α-alumina and Na_2O, but α-alumina did remain when the polymer particle was not added to alumina, but when the polymer was added, the residual α-alumina decreases. It is noted

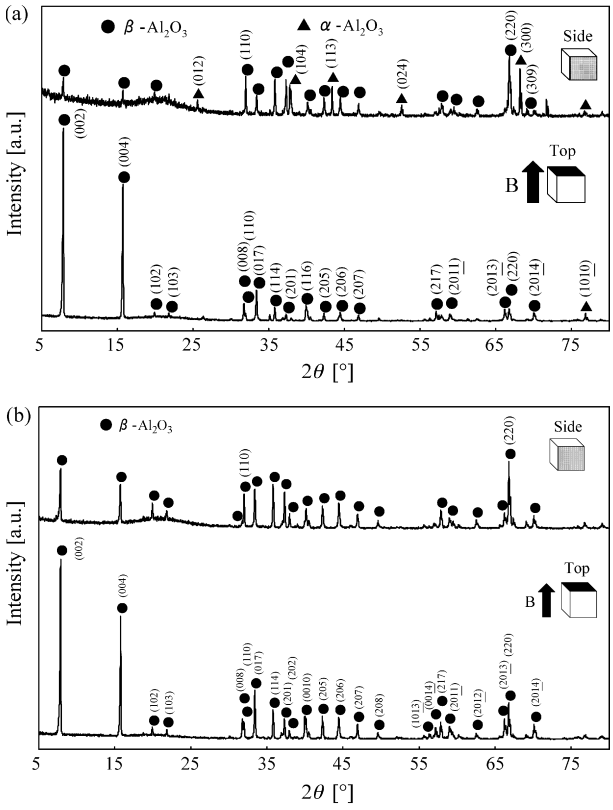

Fig. 2. XRD patterns of reaction-sintered bodies at 1973 K without polymer addition (a) and with polymer addition (b).

that the amount of remaining α-alumina decreased and single-phase β-alumina was prepared for the samples with polymer addition. From Fig. 2, it appears that on the top plane perpendicular to the magnetic field, the diffraction peaks of the (0 0 4) and (0 0 8) (β-alumina) and (1 0 1 0) (α-alumina) planes at the interplanar angle of 17.5° with the basal plane are very large. In contrast, on the side plane parallel to the magnetic field, the peaks of the (1 1 0) and (2 2 0) (β-alumina) and (3 0 0) (α-alumina) planes are very large. These results indicate that a crystalline texture with the *c*-axis perpendicular to the magnetic field was developed by slip casting in the high-magnetic field followed by reaction sintering. Comparing Fig. 2(a) with (b), however, the orientation of the samples with polymer addition is lower than that without polymer addition. This result is interpreted as follows: the addition of polymer to the α-alumina suspension increases the viscosity which results in preventing rotation of the α-alumina particle under a high-magnetic field. The ionic conductivity determined at 473 K of the β-alumina including α-alumina prepared without polymer was negligible, but textured β-alumina shows anisotropic ionic conductivity depending on the crystal orientation.

The ionic conductivity at 473 K of the textured β-alumina was $7.1 \times 10^{-3}\ \Omega^{-1}\ cm^{-1}$ on the side plane and 5.6×10^{-3} on the top plane. The conductivity on the side plane is larger than reported polycrystal conductivity[25] but smaller than single crystal one,[26] which indicates that the texture development is not enough and further optimization research is necessary.

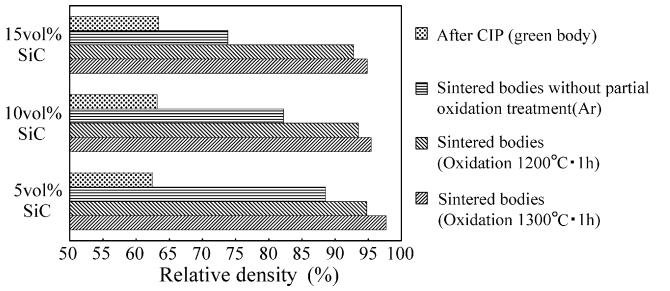

Fig. 3. Relative densities of green bodies after CIP treatment and sintered bodies with oxidation treatment and without oxidation treatment.

3.2. Textured alumina–mullite–SiC nanocomposite

It was clarified that surface SiO_2 of SiC particle and Al_2O_3 react into mullite phase and small amount of SiC remain after partial oxidation at 1573 K followed by sintering at 1873 K. By TEM observation, the existence of dispersed nano-sized SiC particles was confirmed in the matrix. These results indicate that a dense Al_2O_3–mullite–SiC nanocomposite without SiO_2 was fabricated by this method.

Fig. 3 shows the relative densities of the green bodies after CIP treatment for the sintered bodies with and without oxidation treatment, followed by sintering in an Ar atmosphere at 1873 K for 2 h. It was confirmed that the relative density of the sintered bodies significantly increased by the oxidation treatment. The sintered density increased with a high-oxidation temperature and with a small SiC content. When a large quantity of SiO_2 was generated at a high-oxidation temperature, densification was enhanced by the viscous sintering of the surface SiO_2 of SiC and Al_2O_3.[31]

Fig. 4 shows X-ray diffraction patterns for 15 vol.% SiC sintered at 1873 K for 2 h after oxidation treatment. In the T plane and S1 plane which are parallel to the direction of magnetic field *n*, the intensities of (1 1 0) are high while the intensities of (0 0 6) are very low. In contrast, in the S2 plane perpendicular to the high-magnetic field direction, the intensity of (1 1 0) is low and the intensity of (0 0 6) is higher than that of T and S1. These results indicate that the *c*-axis of the alumina crystal was aligned in the high-magnetic field direction. Here, the degree of crystalline texture (*P*) was determined using the following

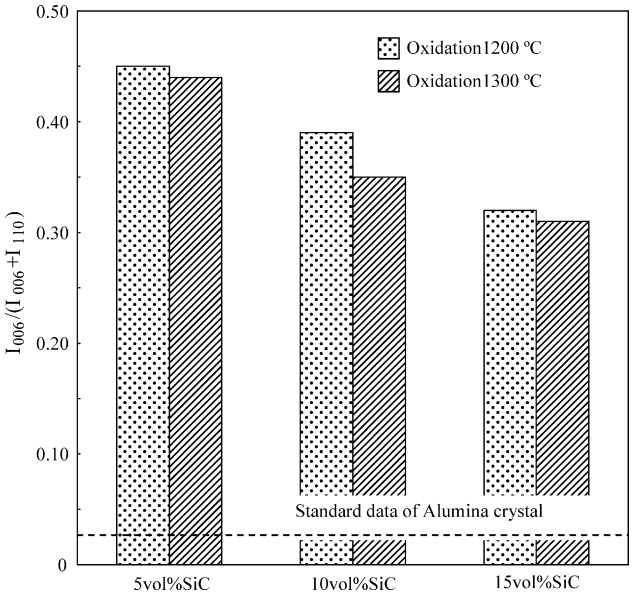

Fig. 5. Degree of crystalline orientation for the specimens prepared by slip casting at 12 T followed by reaction sintering.

equation:

$$P = \frac{I_{006}}{I_{006} + I_{110}} \quad (2)$$

where I_{006} and I_{110} are the X-ray diffraction intensities from the 0 0 6 and the 1 0 0 reflections on the bottom surface, respectively.

Fig. 5 illustrates the degree of crystalline texture for the specimens prepared by slip casting at 12 T after reaction sintering under different oxidation conditions. The degree of crystalline texture significantly increased when the SiC content was low and the oxidation treatment temperature was 1473 K. It is seen that the degree of crystalline texture depended on the Al_2O_3 content but not as high in comparison with the single phase of Al_2O_3.[5,6]

Fig. 6 shows the bend strength for the textured nanocomposite with different directions. From the SEM observations, it is seen that inter-granular fracture was observed in the fracture form but that no significant difference between the fracture surfaces was observed for the different directions of the applied magnetic field. The effect of the alumina orientation on the fracture strength was not clearly observed. This is because

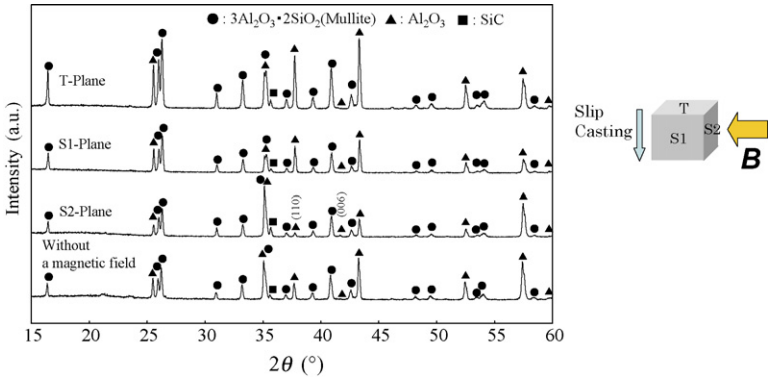

Fig. 4. X-ray diffraction patterns for 15 vol.% SiC sintered at 1873 K for 2 h in an Ar atmosphere after oxidation treatment at 1573 K for 1 h in an O_2 atmosphere, where slip casting was conducted without magnetic field and in 12 T.

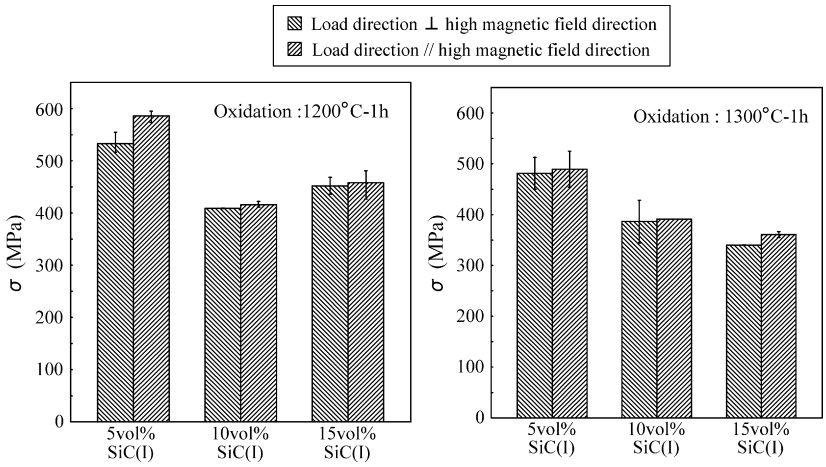

Fig. 6. Three-point bending strength for bodies sintered of the nanocomposites.

the temperature of the reaction sintering was 1873 K and the grain growth of alumina was not significant in this experiment. The fracture strengths decreased with increased SiC (i.e., mullite) contents. The decrease in the fracture strength was due to the content of mullite in sintered bodies because the fracture strength of mullite is not very high at room temperature (300–400 MPa). However, the absolute value of the bend strength was not large in comparison with the data of the highly textured alumina sintered at 1873 K shown in Fig. 7. It is noted for the textured undoped alumina that the bending strength of the plane where load direction parallel to applied magnetic direction is larger than that load direction is perpendicular to magnetic field direction. To clarify the reason of the poor strength especially added large amount of SiC, EDS mapping images were observed for Si and Al. Agglomeration of Si was observed, which indicates that ultrasonic irradiation was not effective for the deagglomeration of SiC powders.

Recently it is clarified that beads-milling using small zirconia beads of 0.05 mm in diameter is effective for the deagglomeration of fine powders.[37] The milling conditions were as follows: the disc rotation speed is 10 m s^{-1} and the milling time is 1 h. Fig. 8 shows that the beads-milling is effective for the deagglomeration of the present suspension system. Smaller media are effective for redispersing agglomerates because the rate of fine grinding is very dependent on the frequency of collisions. Using the beads-milling treated suspensions, the fracture strength increased to above 750 MPa for 10 vol.% SiC systems as is shown in Fig. 9. The bending strength of the plane where load direction parallel to applied magnetic direction is larger than that load direction is perpendicular to magnetic field direction. Similar trend was also observed for undoped alumina ceramics (Fig. 7).

3.3. Electrophoretic deposition in high-magnetic field

Fig. 10 shows the variation in the XRD patterns of the top planes with the angle between the directions of **B** and **E**, where the α-alumina (particle size of 0.2 μm) was deposited in 10 T followed by sintering at 1873 K. The Φ_{hkl} of the appeared

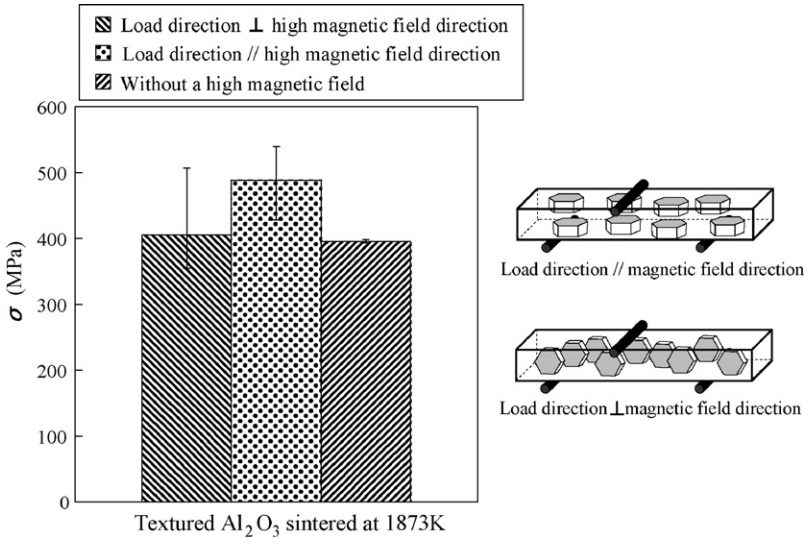

Fig. 7. Three-point bending strength of textured alumina sintered at 1873 K depending on the orientation direction.

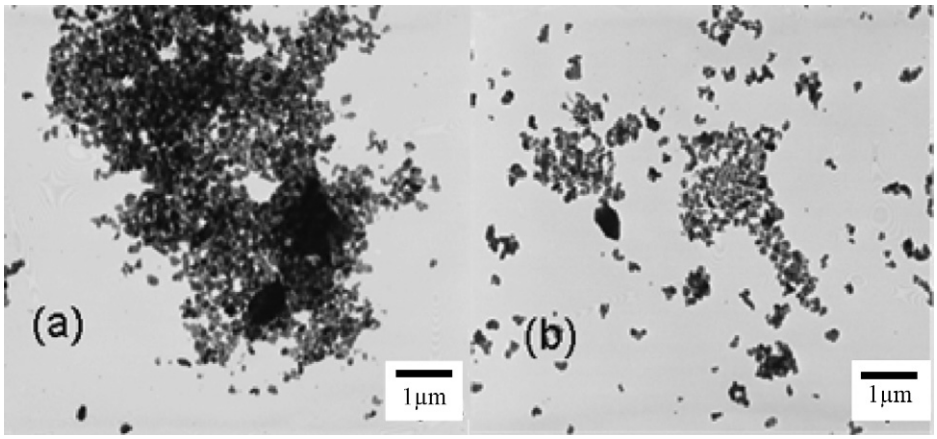

Fig. 8. TEM images of 10 vol.% SiC system before (a) and after (b) beads-milling.

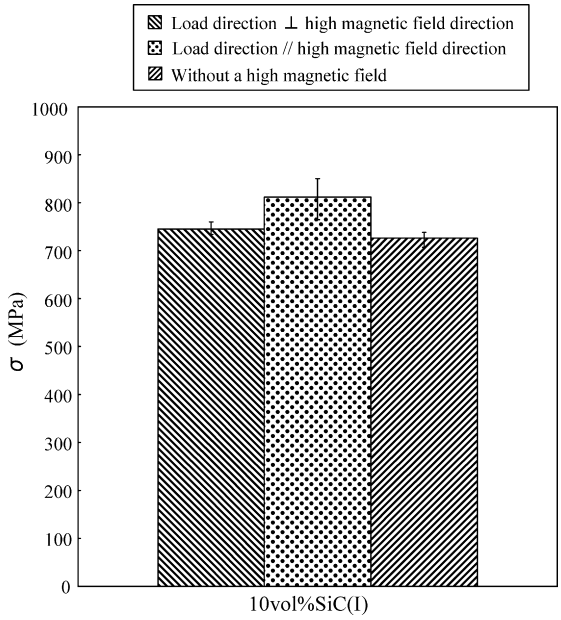

Fig. 9. Three-bending strength of reaction-sintered 10 vol.% SiC systems after milling treatment.

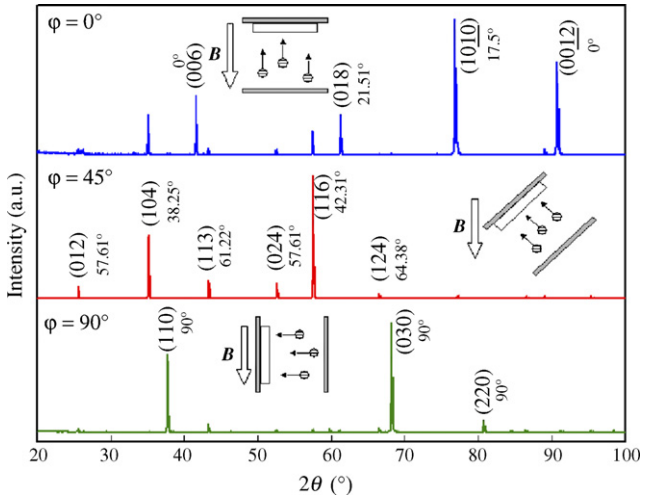

Fig. 10. Changes in the XRD patterns of the top planes with the angle between the direction of **B** and **E**.

peaks are also shown in the figure. When the **E** is parallel to **B** ($\phi_{B-E} = 0°$), the diffraction peaks of the planes at low interplanar angles (Φ_{hkl} is close to 0°) are predominant. When the Φ_{hkl} is changed to 45°, the dominant diffraction peaks change to the planes of the intermediate interplanar angles (ϕ_{B-E} is close to 45°). When **E** is perpendicular to **B** ($\phi_{B-E} = 90°$), the dominant diffraction peaks changed to the planes of high-interplanar angles (Φ_{hkl} is close to 90°). These results clearly show that the dominant crystal faces can be controlled by varying the angle of **E** and **B**.[21,39,40]

Fig. 11 shows an example of textured laminated alumina prepared by EPD in high-magnetic field. Here, the cross-sectional microstructure was prepared by alternately changing $\phi_{B-E} = 0°/90°$ layer by layer. It is seen that microstructure well-reflects the alteration of ϕ_{B-E} during the deposition. The three-point bending strength was measured for the samples with alternately changing $\phi_{B-E} = +45°/-45°$ layer by layer where the tensile surface was either parallel or perpendicu-

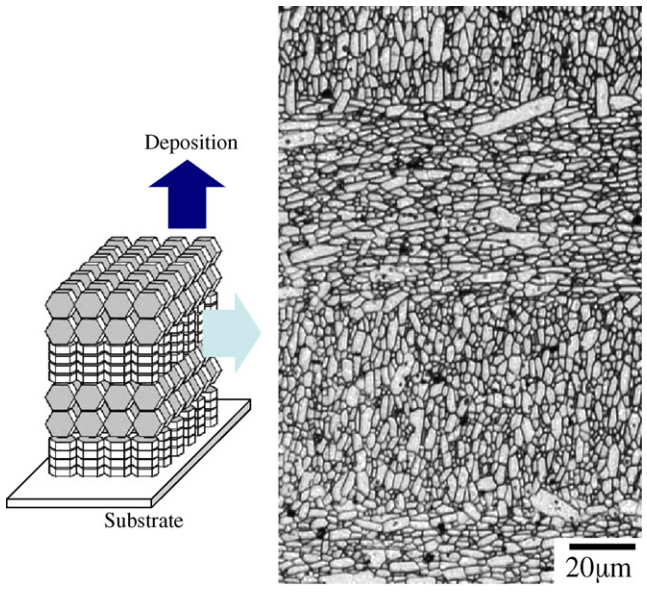

Fig. 11. Cross-sectional microstructure of laminar composite prepared by changing $\phi_{B-E} = 0°/90°$ layer by layer.

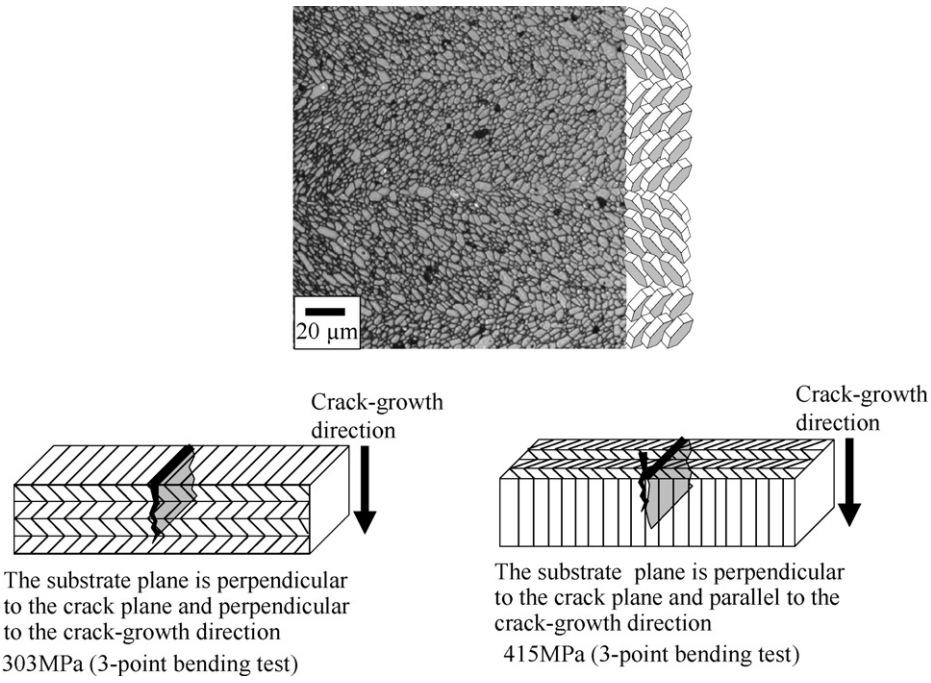

Fig. 12. Bending strength for textured alumina laminate depending on the crack-growth direction and schematic illustrations of crack-growth for bend-bar geometries for textured laminates with alternate orientation.

lar to the plane defined by the EPD direction. A typical SEM microstructure and schematic illustrations of the orientation of the crack-growth relative to the samples are shown in Fig. 12. The strength for the crack-growth direction perpendicular to the deposition direction was higher than that parallel to the deposition direction. The crack was propagated by bending in a zigzag path along the aligned grains when the crack-growth direction was parallel to the deposition direction. The combination of the orientation and lamination is one of the possible ways of tailoring the microstructure for the improvement of mechanical, dielectric, thermo-electric properties, etc.[41,42]

4. Conclusions

Textured ceramics with complicated structures of β-alumina and Al_2O_3–mullite–SiC nanocomposite were fabricated by slip casting in a high-magnetic field followed by reaction sintering. Both showed anisotropic ionic conductivity and bending strength depending on the crystal plane, respectively. The textured laminated alumina was fabricated by EPD in a high-magnetic field alternately changing the direction of the electric field relative to the magnetic field.

Acknowledgement

This study was supported in part by the Budget for Nuclear Research of the Japanese Ministry of Education, Culture, Sports, Science and Technology.

References

1. Messing, G. L., Trolier-McKinstry, S., Sabolsky, E. M., Duran, C., Kwon, S., Brahmaroutu, B. *et al.*, Templated grain growth of textured piezoelectric ceramics. *Crit. Rev. Solid State Mater. Sci.*, 2004, **29**, 45–96.
2. Hirao, K., Ohashi, M., Brito, M. E. and Kanzaki, S., Processing strategy of producing highly anisotropic silicon nitride. *J. Am. Ceram. Soc.*, 1995, **78**, 1687–1690.
3. Takenaka, T. and Sakata, T., Grain orientation and electrical properties of hot-forged $Bi_4Ti_3O_{12}$ ceramics. *Jpn. J. Appl. Phys.*, 1980, **19**, 31–39.
4. Yoshizawa, Y., Toriyama, M. and Kanzaki, S., Fabrication of textured alumina by high-temperature deformation. *J. Am. Ceram. Soc.*, 2001, **84**, 1392.
5. Suzuki, T. S., Sakka, Y. and Kitazawa, T., Orientation amplification of alumina by colloidal filtration in a strong magnetic field and sintering. *Adv. Eng. Mater.*, 2001, **3**, 490–492.
6. Sakka, Y. and Suzuki, T. S., Textured development of feeble magnetic ceramics by colloidal processing under high-magnetic field. *J. Ceram. Soc. Jpn.*, 2005, **113**, 26–36.
7. Uyeda, C., Rotational motion of inorganic diamagnetic crystals induced in the magnetic field. *Jpn. J. Appl. Phys. Part 2*, 1993, **32**, L268–L270.
8. Uyeda, C., Abe, T. and Takashinia, R., Magnetic anisotropy of ordinary crystals without spontaneous magnetic moments detected by rotational oscillations induced by a field of a horseshoe magnet. *Jpn. J. Appl. Phys. Part 2*, 2006, **45**, L268–L271.
9. Sakka, Y., Fabrication of highly microstructure controlled ceramics by novel colloidal processing. *J. Ceram. Soc. Jpn.*, 2006, **114**, 371–376.
10. Inoue, K., Sassa, K., Yokogawa, Y., Sakka, Y., Okida, M. and Asai, S., Control of crystal orientation of hydroxyapatite by imposition of a high-magnetic field. *Mater. Trans.*, 2003, **44**, 1133–1137.
11. Makiya, A., Kusano, D., Tanaka, S., Uchida, N., Uematsu, K., Kimura, T. *et al.*, Particle oriented bismuth titanate ceramics made in high-magnetic field. *J. Ceram. Soc. Jpn.*, 2003, **111**, 702.
12. Suzuki, T. S. and Sakka, Y., Preparation of oriented bulk 5 wt% Y_2O_3–Al_2O_3 ceramics by slip casting in a high-magnetic field and sintering. *Scripta Mater.*, 2005, **52**, 583–586.

13. Wu, C. Y., Li, S. Q., Sassa, K., Sakka, Y., Suzuki, S. T. and Asai, S., The crystal orientation taking account of gravity force under high-magnetic field. *ISIJ Int.*, 2005, **45**, 997–1000.
14. Iwai, K., Akiyama, J., Sun, M. G. and Asai, S., Application of a strong magnetic field on materials fabrication and experimental simulation. *Sci. Technol. Adv. Mater.*, 2006, **7**, 365–368.
15. Zhu, X. W., Suzuki, T. S., Uchikoshi, T., Nishimura, T. and Sakka, Y., Texture development in Si_3N_4 ceramics by magnetic field alignment during slip casting. *J. Ceram. Soc. Jpn.*, 2006, **114**, 979–987.
16. Tabara, K., Makiya, A., Tanak, S., Uematsu, K. and Doshida, Y., Particle oriented strontium bismuth titanate ceramics prepared by using high-magnetic field and subsequent reaction sintering. *J. Ceram. Soc. Jpn.*, 2007, **115**, 237–240.
17. Kaga, H., Kinemuchi, Y., Tanaka, S., Makiya, A., Kato, Z., Uematsu, K. *et al.*, Fabrication of *c*-axis oriented $Zn_{0.98}A_{l0.02}O$ by a high-magnetic-field via gelcasting and its thermoelectric properties. *J. Ceram. Soc. Jpn.*, 2006, **114**, 1085–1088.
18. Sakka, Y., Takahashi, K., Suzuki, T. S., Ito, S. and Matsuda, N., Texture development of hydroxyapatite ceramics by colloidal processing in a high-magnetic field followed by sintering. *Mater. Sci. Eng. A*, 2008, **475**, 27–33.
19. Yamauchi, Y., Sawada, M., Sugiyama, A., Osaka, T., Sakka, Y. and Kuroda, K., Magnetically induced orientation of mesochannels in 2D-hexagonal mesoporous silica films. *J. Mater. Chem.*, 2006, **16**, 3693–3700.
20. Guilmean, E., Chateigner, D., Suzuki, T. S., Sakka, Y. and Henrist, C., Rietveld texture analysis of alumina ceramics by neutron diffraction. *Chem. Mater.*, 2005, **17**, 102–106.
21. Suzuki, T. S., Uchikoshi, T. and Sakka, Y., Control of texture in alumina by colloidal processing in a strong magnetic field. *Sci. Technol. Adv. Mater.*, 2006, **7**, 356–364.
22. Kimura, M., Shiratsuyu, K., Ando, A., Suzuki, T. S. and Sakka, Y., Layer structure of textured $CaBi_4Ti_4O_{15}$ ceramics fabricated by slip casting in high-magnetic field. *J. Am. Ceram. Soc.*, 2007, **90**, 1463–1466.
23. Suzuki, T. S., Sakka, Y. and Kitazawa, K., Preferred orientation of the texture in the SiC whisker-dispersed Al_2O_3 ceramics by slip casting in a high-magnetic field. *J. Ceram. Soc. Jpn.*, 2001, **109**, 886–890.
24. Suzuki, T. S., Uchikoshi, T. and Sakka, Y., Texture development in alumina composites by slip casting in a strong magnetic field. *J. Ceram. Soc. Jpn.*, 2006, **114**, 59–62.
25. Hirata, Y., Lee, S. Y., Shimada, K. and Ishihara, Y., Electrical properties of MgO-doped beta alumina ceramics prepared from the metal alkoxides Nippon Seramikkusu Kyokai Gakujutsu Ronbunshi. *J. Ceram. Soc. Jpn.*, 1992, **100**, 877–881.
26. Fielder, W. L., Kautz, H. E., Ford, J. S. and Singer, J., Conductivity of boules of single-crystal sodium beta-alumina. *J. Electrochem. Soc.*, 1975, **122**, 528–530.
27. Dogotsi, G. A., Fracture toughness of ceramics and ceramic composites. *Ceram. Int.*, 2003, **29**, 777–784.
28. Yoshizawa, Y., Hirao, K. and Kanzaki, S., Fabrication of low cost fine-grained alumina powders by seeding for high performance sintered bodies. *J. Eur. Ceram. Soc.*, 2004, **24**, 325–330.
29. Osendi, M. I. and Baudin, C., Mechanical properties of mullite materials. *J. Eur. Ceram. Soc.*, 1996, **16**, 217–224.
30. Ohira, H. M. M., Ismail, G., Yamamoto, U., Akiba, Y. and Somiya, T. S., Mechanical properties of high-purity mullite at elevated temperatures. *J. Eur. Ceram. Soc.*, 1996, **16**, 225–229.
31. Sakka, Y., Bidinger, D. D. and Aksay, I. A., Processing of silicon carbide–mullite–alumina nanocomposite. *J. Am. Ceram. Soc.*, 1995, **78**, 479–486.
32. Hirata, Y., Izaiku, T. and Ishihara, Y., Synthesis of dense beta, beta″-alumina ceramics by reaction sintering of Na_2O-containing alumina compact. *J. Mater. Res.*, 1991, **6**, 585–591.
33. Sakka, Y., Honda, A., Suzuki, T. S. and Moriyosh, Y., Fabrication of oriented β-alumina from porous bodies by slip casting in a high-magnetic field. *Solid State Ionics*, 2004, **172**, 341–347.
34. Tang, F. Q., Fudouzi, H., Uchikoshi, T. and Sakka, Y., Preparation of porous materials with controlled pore size and porosity. *J. Eur. Ceram. Soc.*, 2004, **24**, 341–344.
35. Sakka, Y., Tang, F. Q., Fudouzi, H. and Uchikoshi, T., Fabrication of porous ceramics with controlled pore size by colloidal processing. *Sci. Technol. Adv. Mater.*, 2005, **6**, 915–920.
36. Suzuki, T. S., Sakka, Y., Nakano, K. and Hiraga, K., Effect of ultrasonication on the microstructure and tensile elongation of zirconia-dispersed alumina ceramics prepared by colloidal process. *J. Am. Ceram. Soc.*, 2001, **84**, 2132–2134.
37. Inkyo, M. and Tahira, T., Dispersion of agglomerated nanoparticles by fine beads mill. *J. Soc. Powder Powder Technol. Jpn.*, 2004, **41**, 578–585 [in Japanese].
38. Uchikoshi, T., Ozawa, K., Hatton, B. D. and Sakka, Y., Dense, bubble-free ceramic deposits from aqueous suspensions by electrophoretic deposition. *J. Mater. Res.*, 2001, **16**, 321–324.
39. Uchikoshi, T., Suzuki, T. S., Okuyama, H. and Sakka, Y., Electrophoretic deposition of alpha-alumina particles in a strong magnetic field. *J. Mater. Res.*, 2003, **18**, 254–256.
40. Uchikoshi, T., Suzuki, T. S., Okuyama, H. and Sakka, Y., Control of crystalline texture in polycrystalline alumina ceramics by electrophoretic deposition in a strong magnetic field. *J. Mater. Res.*, 2004, **19**, 1487–1491.
41. Okamoto, T., Horii, S., Uchikoshi, T., Suzuki, T. S., Sakka, Y., Funahashi, R. *et al.*, Fabrication of multilayered oxide thermoelectric modules by electrophoretic deposition under high-magnetic fields. *Appl. Phys. Lett.*, 2006, **89** [Art. No. 081912].
42. Horii, S., Kumagai, T., Uchikoshi, T., Suzuki, T. S., Sakka, Y., Shimoyama, J. I. *et al.*, Improvement of thermoelectric performance in magnetically *c*-axis-oriented bismuth-based vobaltite. *Scripta Mater.*, 2007, **57**, 333–336.